Carbon 228 (2024) 119374

Contents lists available at ScienceDirect

Carbon

journal homepage: www.elsevier.com/locate/carbon

High-pressure dysprosium carbides containing carbon dimers, trimers, chains, and ribbons

Fariia Iasmin Akbar [a,b,*], Alena Aslandukova [a], Yuqing Yin [b,c], Andrey Aslandukov [a,b], Dominique Laniel [d], Elena Bykova [e], Maxim Bykov [f], Eleanor Lawrence Bright [g], Jonathan Wright [g], Davide Comboni [g], Michael Hanfland [g], Natalia Dubrovinskaia [b,c], Leonid Dubrovinsky [a,**]

[a] Bavarian Research Institute of Experimental Geochemistry and Geophysics (BGI), University of Bayreuth, Univesitaetsstrasse 30, 95440, Bayreuth, Germany
[b] Material Physics and Technology at Extreme Conditions, Laboratory of Crystallography, University of Bayreuth, Univesitaetsstrasse 30, 95440, Bayreuth, Germany
[c] Department of Physics, Chemistry and Biology (IFM), Linköping University, SE-581 83, Linköping, Sweden
[d] Centre for Science at Extreme Conditions and School of Physics and Astronomy, University of Edinburgh, EH9 3FD, Edinburgh, United Kingdom
[e] Institute of Geosciences, Goethe University Frankfurt, Altenhöferallee 1, 60438, Frankfurt Am Main, Germany
[f] Institute of Inorganic and Analytical Chemistry, Goethe University Frankfurt, Max-von-Laue-Straße 7, 60438, Frankfurt Am Main, Germany
[g] European Synchrotron Radiation Facility, CS 40220, 38043 Grenoble Cedex 9, France

ARTICLE INFO

Keywords:
High-pressure
Diamond anvil cell
Rare-earth carbides
Carbides
Rare-earth elements
Dysprosium carbide

ABSTRACT

Exploring the chemistry of materials at high pressure leads to discoveries of previously unknown compounds and phenomena. Here chemical reactions between elemental dysprosium and carbon were studied in laser-heated diamond anvil cells at pressures up to 95 GPa and temperatures of ~2800 K. *In situ* single-crystal synchrotron X-ray diffraction (SCXRD) analysis of the reaction products revealed the formation of novel dysprosium carbides, γ-DyC_2, Dy_5C_9, and γ-Dy_4C_5, along with previously reported Dy_3C_2 and Dy_4C_3. The crystal structures of γ-DyC_2 and Dy_5C_9 feature infinite flat carbon polyacene-like ribbons and *cis*-polyacetylene-type chains, respectively. In the structure of γ-Dy_4C_5, carbon atoms form dimers and non-linear trimers. Dy_3C_2 contains ethanide-type carbon dumbbells, and Dy_4C_3 is methanide featuring single carbon atoms. Density functional theory calculations reproduce well the crystal structures of high-pressure dysprosium carbides and reveal conjugated π-electron systems in novel infinite carbon polyanions. This work demonstrates that complex carbon homoatomic species previously unknown in organic chemistry can be synthesized at high pressures by direct reactions of carbon with metals.

1. Introduction

The chemistry of binary compounds drastically changes and expands at high pressures. Recent striking examples include the synthesis of novel polyhalides [1,2], polynitrides [3–10], polyborides [11,12], polyhydrides [13–15], whose structures possess various homonuclear chemical species, such as dimers, trimers, pentagonal and hexagonal rings, polymeric chains, atomic layers and 3D networks previously unobserved in binary compounds at ambient pressures. The observed tendency of forming homonuclear chemical bonds is well understood by theory [16]: in very general terms, with increasing pressure the distances between atoms decrease and the value of resonance integrals increases, resulting in a larger gap between bonding and antibonding states and stronger bonds. Modern *a priori* structure prediction techniques, however, are not precise enough to provide an exhaustive list of possible chemical compositions and phases at given thermodynamic conditions. Even moderate-pressure experiments report phases and crystal structures never predicted or previously considered [1,4,5,8,13].

Homonuclear chemical bonding between carbon atoms is at the heart of organic chemistry and the number of arrangements for carbons connections (or catenation) known at ambient pressure is enormous. Strikingly, recent experimental observations indicate that carbon polyanions in metal carbides at high pressures may be unknown and even not foreseen at ambient pressure. For example, novel yttrium carbide γ-Y_4C_5

* Corresponding author.
** Corresponding author.
E-mail addresses: Fariia.Akbar@uni-bayreuth.de (F.I. Akbar), Leonid.Dubrovinsky@uni-bayreuth.de (L. Dubrovinsky).

https://doi.org/10.1016/j.carbon.2024.119374
Received 16 April 2024; Received in revised form 18 June 2024; Accepted 19 June 2024
Available online 19 June 2024

at 44–51 GPa possesses significantly bent carbon trimers [C_3] isoelectronic with ozone O_3 [17]. Polycarbides of different compositions have been claimed in the Li–C system: due to the polymerization of Li_2C_2 acetelenide upon compression [18] or formation of LiC_2 graphenide and Li_3C_4 polyacenide [19] after laser heating. Beyond these, theoretical calculations for metal carbides at high pressure predict carbon polyanions with unusual geometry and chemical bonding [20–22], for example, in numerous polycarbides in the Ca–C, Y–C and Th–C systems [20,22–27]. Some of these novel carbon compounds are expected to have quite exotic structures, in which carbon atoms are polymerized to form infinite quasi-1D ribbons built of fused six-membered rings, and the synthesis of high-pressure CaC_2 phase (HP–CaC_2) with polyacene-like ribbons was recently reported [28]. All these predictions and discoveries call for systematic experimental studies of high-pressure carbides.

Recently, we reported the synthesis of Dy_3C_2 and Dy_4C_3 at high temperatures and pressures below ~58 GPa [29]. Here we have extended the pressure range up to 95 GPa and report the results of our systematic high-pressure high-temperature (HPHT) investigations of the Dy–C system using laser-heated diamond anvil cells (DACs).

2. Materials and methods

Nomenclature

For the sake of clarity for readers, in this paper we use simplified nomenclature of anionic units in the crystal structures of Dy–C compounds. In particular, if not specified otherwise we will mean completely deprotonated species. So, by using the term ethanide, we will mean ethanehexaide C26-. Polyacetylide stands for fully deprotonated polyacetylene poly-[ethene-1,2-diyl]. Polyacenide is derived by full deprotonation of polyacene or poly(buta-1,3,-diene-1,4:3,2-tetrayl).

2.1. Sample preparation

In our experiments, we used BX90-type diamond anvil cells with a large X-ray aperture [30]. As anvils, we employed Boehler−Almax-type diamonds with culets diameter of 80/120 μm. Rhenium gaskets with an initial thickness of 200 μm were indented to ~16/22 μm and a hole of ~35/55 μm laser-drilled in the center of the indentation. The dysprosium (99.9 % purity, Merc Inc.) flakes were loaded between one of the diamonds and a layer of dry sodium chloride (99.999 % purity, ChemPUR) that played a role of a thermal insulator and pressure transmitting medium; diamond anvils were used as a carbon source. Samples were compressed to the desired pressure and laser-heated up to ~2800 K. Laser heating of the samples was carried out using an *in house* double-sided YAG laser (1064 nm wavelength) heating setup [31]. Thermal emission spectra from the heated area were collected via IsoPlane SCT 320 spectrometer with a 1024 × 2560 PI-MAX 4 camera [31]. The pressure was determined using the NaCl equation of states (EoS) [32,33].

2.2. X-ray diffraction

The reaction products were analyzed by single-crystal X-ray diffraction measurements at the two synchrotron beamlines: ID11 of ESRF, Grenoble, France ($\lambda = 0.2846$ Å, beam size ~ 0.75 × 0.75 μm^2); ID15B of ESRF, Grenoble, France ($\lambda = 0.4100$ Å, beam size ~1.5 × 2 μm^2). Powder XRD images were collected upon continuous rotation of the sample in a range ±1° around the vertical ω axis at ESRF. During single-crystal collection, the cell was rotated from −38° to +38° with narrow 0.5° steps. Creating maps with XDI software [34] helps to visualize the phase distribution within the pressure chamber and to locate areas where the step-scans should be performed. The CrysAlis^{Pro} software package [35] was used for the analysis of the single-crystal XRD data (peak hunting, indexing, data integration, frame scaling, and absorption correction). To calibrate an instrument model in the CrysAlis^{Pro} software, i.e. the sample-to-detector distance, detector's origin, offsets of the goniometer angles, and rotation of both the X-ray beam and detector around the instrument axis, we used a single crystal of orthoenstatite [$(Mg_{1.93}Fe_{0.06})(Si_{1.93},Al_{0.06})O_6$, *Pbca* space group, a = 8.8117(2) Å, b = 5.18320(10) Å, and c = 18.2391(3) Å]. The DAFi program was used for the search of reflection's groups belonging to the individual single crystal domains [36]. Using the OLEX2 software package [37], the structures were solved with the ShelXT structure solution program [38] using intrinsic phasing and refined with the ShelXL [39] refinement package using least-squares minimization. Crystal structure visualization was made with the VESTA software [40]. The equations of state were obtained by fitting the pressure-volume dependence data using the EoSFit7-GUI [41].

Accurate determination of the positions of light carbon atoms in the presence of heavy dysprosium atoms is challenging. In order to improve both precision and accuracy in determining C–C distances, 12 to 27 domains with $R_{int} < 5$ % and $R_1 < 8$ % for each of the studied carbides were identified, their structures were refined, and C–C distances for each corresponding domain were averaged. That allows reduce the standard error of C–C distances to smaller than 0.009 Å, and the corresponding data presented in the main text of the paper.

2.3. Theoretical calculations

The properties of the synthesized compounds were determined through the first-principles calculations using the framework of density functional theory (DFT) as implemented in the VASP (Vienna *ab initio* simulation package) code [42]. To expand the electronic wave function in plane waves we used the Projector-Augmented-Wave (PAW) method [43]. The Generalized Gradient Approximation (GGA) functional was used for calculating the exchange-correlation energies, as proposed by Perdew–Burke–Ernzerhof (PBE) [44]. The PAW potentials with the following valence configurations of 5s5p6s5d for Dy ("Dy_3") and 2s2p for C ("C") were used to describe the interaction between the core and the valence electrons in frozen f-electrons approximation for Dy [42]. Convergence tests with a threshold of 1 meV per atom in energy led to an energy cutoff for the plane wave expansion of 750 eV for all phases and a Monkhorst-Pack [45] k-point grid of 15 × 7 × 6 for γ-DyC_2, 4 × 4 × 6 for Dy_5C_9, 3 × 5 × 4 for γ-Dy_4C_5, 6 × 6 × 11 for Dy_3C_2, and 4 × 4 × 4 for Dy_4C_3. Computations were performed for eight volumes that cover the pressure range of 0–100 GPa. Harmonic lattice dynamics calculations were performed with the PHONOPY software [46] using the finite displacement method for 3 × 3 × 3 (γ-DyC_2), 2 × 2 × 3 (Dy_5C_9), 2 × 2 × 2 (γ-Dy_4C_5), 2 × 2 × 3 (Dy_3C_2) and 2 × 2 × 2 (Dy_4C_3) supercells with respectively adjusted k-points. The tetrahedron method was used for Brillouin zone integrations, employing a mesh of 16 × 16 × 16 k-points for γ-DyC_2, 8 × 8 × 12 k-points for Dy_5C_9, 10 × 10 × 8 k-points for γ-Dy_4C_5, 12 × 12 × 22 k-points for Dy_3C_2 and 8 × 8 × 8 k-points for Dy_4C_3 [47,48]. The integrated values of the crystal orbital bond index (ICOBI) [49] and Mulliken charges were calculated using LOBSTER v4.1.0 software [50]. The charge distribution in the ionic approximation based on a generalization of Pauling's concept of bond strength [51] was made using CHARDI2015 [52]. In our calculations, temperature, configurational entropy, and the entropy contribution due to lattice vibrations were neglected.

3. Results and discussion

A summary of our experiments is presented in Table S1. High-pressure reactions between dysprosium and carbon in DACs at pressures of ~70 and ~95 GPa and temperatures of ~2800 K resulted in the formation of five dysprosium carbides, namely γ-DyC_2, Dy_5C_9, γ-Dy_4C_5, Dy_3C_2, and Dy_4C_3 (Table S2). The first three are novel polycarbides. The full crystallographic datasets for all compounds were deposited to the Cambridge Structural Database (CSD), the Cambridge Crystallographic

Data Centre (CCDC) [53], and their deposition numbers are provided in the corresponding Tables in Supporting Information. The reconstructed reciprocal lattice planes obtained upon processing the synchrotron single-crystal XRD for all synthesized phases are shown in Fig. S1.

The DyC_2 phase synthesized at ~70 GPa has a crystal structure different from that of the two previously known DyC_2 polymorphs, α-DyC_2 (CaC_2-type structure, tetragonal space group *I*4/*mmm*) [54] and β-DyC_2 (KCN-type structure, cubic space group *Fm*-3*m*) [55,56]. Naturally, we named it γ-DyC_2. The γ-DyC_2 phase (space group *Immm*, #71, *Z* = 4, Tables S2 and S3) is isostructural to the previously observed HP-CaC_2 (*Immm*) [28] and the predicted YC_2 (*Immm*) [23]. Its orthorhombic unit cell contains four dysprosium atoms occupying the Wyckoff site 4*i* and eight carbon atoms occupying two distinct crystallographic positions: C1 – 4*h* and C2 – 4*g* (Fig. 1, Table S3).

In the structure of γ-DyC_2 (Fig. 1, Tables S2 and S3), dysprosium atoms form distorted, slightly buckled closed packed layers in the (0 0 1) plane (Fig. 1b). Dysprosium atoms have 12 carbon neighbors arranged in a hexagonal prism with unequal bases (Fig. 1c). Carbon atoms lie in the (0 0 2) plane in the middle between planes of Dy atoms (Fig. 1). They are arranged in polymerized hexagonal rings – flat one-dimensional ribbons propagating along the [1 0 0] direction (Fig. 1). Thus, the carbon atoms form exotic $^{1}_{\infty}[C_4]$ one-dimensionally infinite polyanions.

The structure of the Dy_5C_9 carbide (space group *P*4/*mnc*, #128, *Z* = 2) (Tables S2 and S4) is unprecedented, for we found neither any structural analogue, nor a relevant prediction from theoretical methods. Its unit cell contains two crystallographically distinct dysprosium atoms (Dy1 and Dy2 occupying 8*h* and 2*b* Wyckoff positions, respectively) and two types of carbon atoms (C1 and C2 occupying 16*i* and 2*a* Wyckoff positions, respectively). Dysprosium atoms form slightly distorted square layers in the (0 0 1) plane at a distance of 1/2*c*; each layer is rotated relatively to an adjacent one by ~40° (Fig. 2b and S2). The distinct dysprosium atoms have different environments – Dy1 atoms are in irregular polyhedra with 11 vertices, while Dy2 atoms are located in bicapped square prisms (Fig. 2c and d). The carbon atoms C2 have isolated positions in the structure like the carbon in methanides (Fig. 2). The C1 carbon atoms form zig-zag chains with four atoms per repeating element (Fig. 2). Chains are propagating along the [0 0 1] direction.

The dysprosium carbide isostructural with the recently discovered γ-Y_4C_5 phase [17] is referred to as γ-Dy_4C_5 (orthorhombic space group *Cmce*, #64, Z = 8) (Tables S2 and S5, Fig. S3). Its structure described previously [17] contains carbon dimers [C_2] (dumbbells) and non-linear trimers [C_3] (the angle ∠(C2–C4–C2) is of ~132°, Fig. S3). Two other carbides observed in this work (Table S2), dysprosium (III) methanide Dy_4C_3, and dysprosium (II) ethanide Dy_3C_2, have been synthesized at ~55 GPa in our previous study [29]. For completeness, their structures at ~70 GPa (Dy_3C_2) and ~95 GPa (Dy_4C_3) are shown in Figs. S4 and S5 and structural data are given in Tables S6 and S7.

The analysis of the chemical nature of the novel dysprosium carbides containing polyanions requires a complex approach, especially because *ab initio* methods (see *Methods* section for details) do not always accurately reproduce experimental observations for the *f*-element Dy [29,57,58]. Therefore, we first conduct the crystal-chemical analysis and then complement the analysis with theoretical calculations for isostructural (experimentally observed or hypothetical) compounds of analogous elements devoid of *f*-electrons (like Ca or Y).

In γ-DyC_2, the carbon ribbons are flat. The C–C distances in the hexagons, refined at 70 GPa, are equal to 1.451(9) Å and 1.508(5) Å for the C2–C2 and C1–C2 bonds, respectively. Two angles in the hexagon are found to be of 122.5(7)°, while the other four angles are of 118.8(3)° (Fig. 1d). The angles are close to 120°, and C–C distances are quite similar indicating the sp^2 hybridisation of carbon atoms. In the ideal polyacene chain with ordered single- and double-order carbon-carbon bonds [59], the distribution of shorter and longer C–C contacts is incompatible with the experimental observations for γ-DyC_2 (and for HP-CaC_2 as well [28]). Similar C–C bond lengths within the hexagons in γ-DyC_2 (and HP-CaC_2) suggest a conjugated *π*-electron system in polyacene-like ribbons. The integrated crystal orbital bond indexes (ICOBI) [49] calculated for γ-DyC_2, HP-CaC_2, and isostructural YC_2 (Table S8) vary from ~0.7 to ~1.0. These values, being sufficiently close to 1, confirm strong covalent bonding between carbon atoms. The ELF maps for γ-DyC_2, HP-CaC_2, YC_2 (Fig. S6) also demonstrate localization of electrons on C–C bonds in hexagons, and ionic bonding between Dy and C units. Calculated electron density of states (eDOSes) (Fig. S6) for these phases show the presence of carbon *p*-electrons at the Fermi level that agrees with the formation of the conducting conjugated *π*-electron system.

According to the experimental data, the length of common edges of hexagons in γ-DyC_2 and HP-CaC_2 is slightly (by ~0.05 Å) shorter than

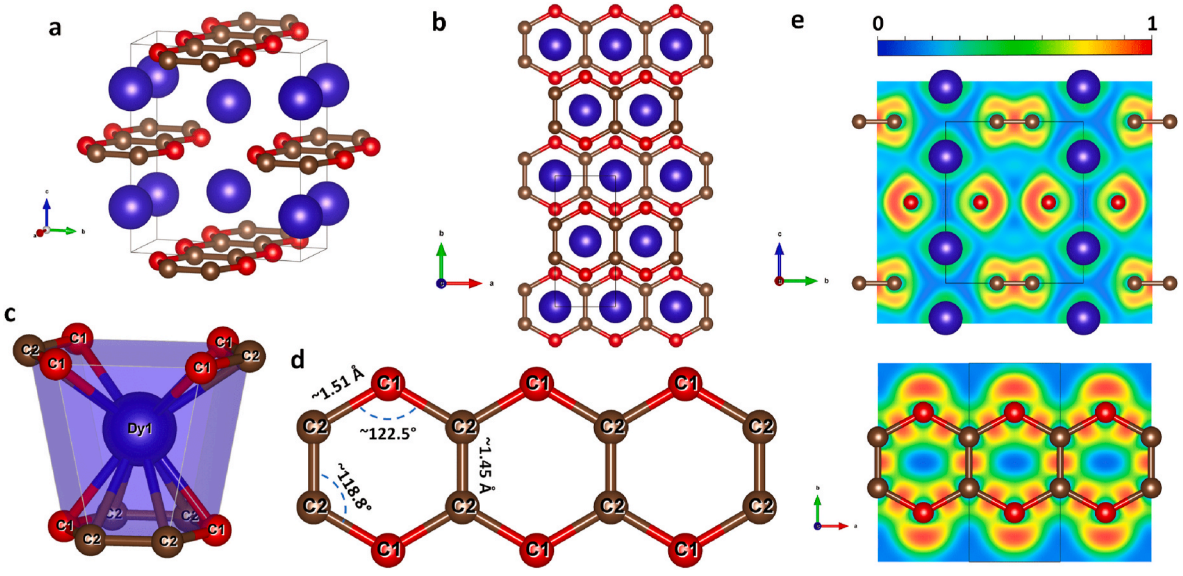

Fig. 1. Crystal structure of DyC_2 at 66(3) GPa. Dy1 atoms are blue, C1 atoms are red, C2 atoms are brown; grey thin lines outline the unit cell. (a) A general view of the crystal structure. (b) The crystal structure viewed along the *c*-axis. (c) The coordination environment of the dysprosium atom. (d) A view of the carbon ribbon. (e) The electron localization function calculated in the (1 0 0) (top) and (0 0 1) plane containing carbon ribbons (bottom). (A colour version of this figure can be viewed online.)

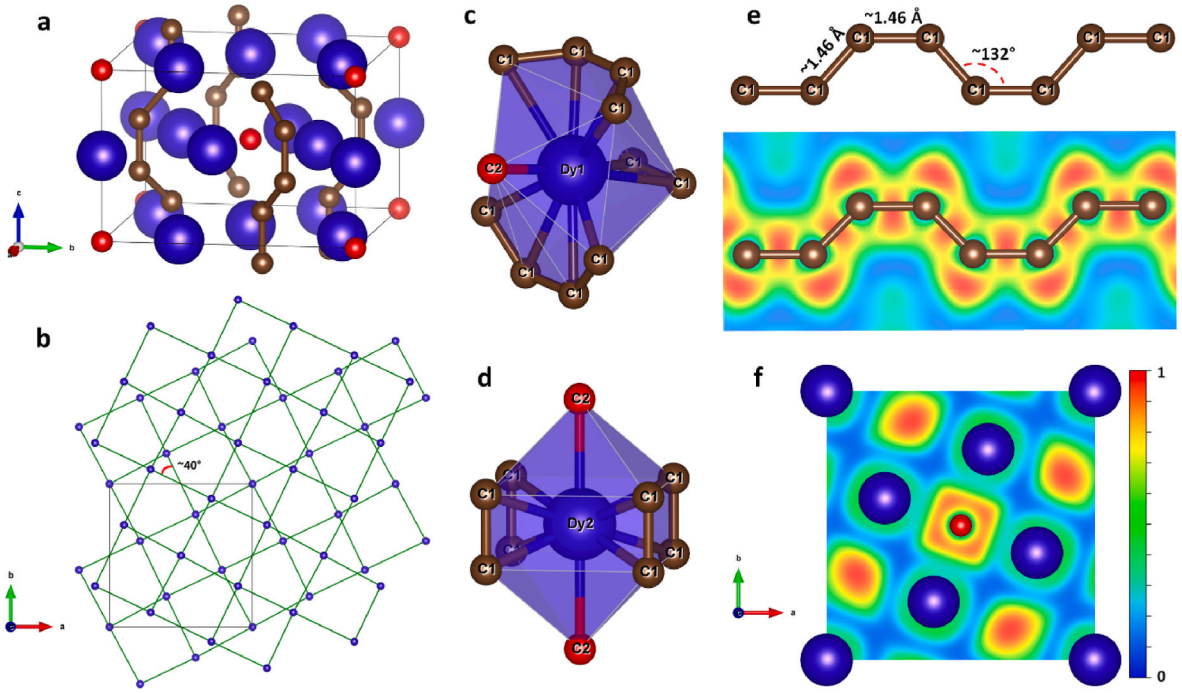

Fig. 2. Crystal structure of Dy_5C_9 at 68(3) GPa. All Dy atoms are blue, C atoms forming chains are brown, discrete C atoms are red; grey thin lines outline the unit cell. (a) A general view of the crystal structure. (b) Arrangement of parallel planes comprised of Dy atoms rotated relative to each other by ~40°. (c) and (d) The coordination environment of the Dy1 and Dy2 atoms. (e) A carbon chain geometry (top) and the electron localization function calculated in the plane containing the carbon chain (bottom). (f) The electron localization function calculated in the (0 0 2) plane. (A colour version of this figure can be viewed online.)

the length of non-shared edges. This agrees with the calculations for all three isostructural high-pressure carbides (DyC_2, CaC_2, and YC_2), which result in the shorter common edges by ~0.02–0.03 Å. This observation is in contrast with what is known for crystals of organic polyaromatic hydrocarbons (naphthalene, anthracene, tetracene, pentacene, pyrene [59–61]) where common edges of hexagon carbon rings are slightly longer (up to ~0.1 Å) than those with carbon connected to hydrogen. A similar effect is known, for example, for acetylene and acetylides [62]. The reason could be the strong electrostatic interaction between carbon and the metal ion: indeed, at ambient pressure, the difference in electronegativity of C and H is ~0.3 eV/e [63–65]. At 70 GPa, this difference significantly increases, reaching ~5.9 eV/e for C and Dy, ~17 eV/e – for C and Ca, and ~15.7 eV/e – for C and Y [64,65]. According to calculations and available experimental data, the average C–C distances in hexagons of γ-DyC_2 and YC_2 (~1.49 Å) are slightly longer than in HP-CaC_2 (~1.45 Å). This qualitatively aligns with some additional electron transfer from cation to carbon ribbons in rare earth carbides in comparison to HP-CaC_2: there is a small decrease of the C–C bond order and higher formal charges on Dy and Y in rare earth carbides than in HP-CaC_2.

According to SCXRD for Dy_5C_9 at ~70 GPa, the C–C distance in the carbon chains is of ~1.46 Å and the C–C–C angle is of ~132°. All atoms of the chain lie in the same plane, as the torsion angle is zero (Fig. 2e). The crystal structure is well reproduced by theoretical calculations (Table S4). According to the theory, both in Dy_5C_9 and in a hypothetical Y_5C_9 with the same structure, the lengths of C–C bonds are very similar (alternating lengths along the chain are of ~1.42 Å and ~1.44 Å at 70 GPa), and the angle between carbon atoms is of ~135°. That implies *cis*-polyacetylene type deprotonated carbon chains with predominantly sp^2-hybridized carbon and conjugated π-electron system. The ICOBI calculated for carbon atoms in the chains of Y_5C_9 and Dy_5C_9, are equal to ~0.7 and ~1.1 respectively. The presence of carbon's *p*-electrons at the Fermi level, as in the calculated eDOS (Fig. S7, Table S8) supports this assignment. Strong covalent bonding between carbon atoms in the chains, and the ionic nature of Dy and isolated C are evident from ELF maps (Fig. 2 and S7). At the same time, C–C distances are significantly longer than in *cis*-polyacetylene – 1.37 Å [66], and the bond angle is significantly larger than 120° expected for sp^2-hybridized carbon. Remarkably, in γ-Dy_4C_5 and γ-Y_4C_5 the geometry of [C_3] groups (in γ-Dy_4C_5, C–C contact is of ~1.43 Å, bond angle – ~132°) is very similar to the geometry of elements forming *cis*-polyacetylene-type chains. Experimental and theoretical data on γ-Y_4C_5 [17] suggest that the bond order of carbon atoms in [C_3] is ~1.31. Thus, carbon chains discovered in Dy_5C_9 can be considered as polymerized in *cis* conformation [C_3] groups found in γ-Dy_4C_5 and γ-Y_4C_5.

As discussed above, the analysis of ELF maps (Figs. 1 and 2, and S3-S7) suggests the ionic bonding between dysprosium and carbon species in γ-DyC_2, Dy_5C_9, γ-Dy_4C_5, and Dy_3C_2. that allows considering them, along with Dy_4C_3, as salt carbides [62]. In fact, the synthesis of all these compounds from elements also makes them similar to salt carbides, so that one can assign a formal charge to a carbon atom or to carbon groups.

There is a correlation between the formal charges of nitrogen and carbon dimers and their lengths. Recently we demonstrated this using as an example $[N_2]^{x-}$ dimers in the high-pressure $Na_3(N_2)_4$, $Ca_3(N_2)_4$, $Sr_3(N_2)_4$, and $Ba(N_2)_3$ compounds [3] and, for $[C_2]^{x-}$ dimers, in yttrium carbide γ-Y_4C_5 containing both [C_2] and nonlinear [C_3] units [17]. In the structures of the carbon compounds synthesized in this study, there are more complex carbon arrangements, including infinite ribbons of fused carbon rings, that imposed a necessity to introduce the effective bond order into consideration to comprehend the relationship between the C–C bond lengths and formal charges of individual carbon atoms or their groups. We have collected the literature data for a number of binary metal-carbon compounds featuring [C_2] or [C_3] units [17,29,54,67–84] with reported C–C interatomic distances. For each of these compounds, we calculated the effective bond order (EBO) between the carbon atoms using two equations introduced below. For a compound containing both isolated "methanide"-type carbon atoms and carbon dimers, with the chemical formula $Me_n(C_2)_mC_k$ (*k* is number of isolated "methanide"-type carbon atoms, and *m* is the number of carbon dimers), the effective bond

order (EBO) between carbon atoms is calculated as follows:

$$EBO = \frac{(2 \times 4m - nZ_{Me} + 4k)}{2m}, \quad (1)$$

where "4" is the number of valence electrons in a free carbon atom, Z_{Me} is the formal charge of the cation. Carbons' formal charge in dimers is $x = 4\text{-}EBO$. For example, for barium acetylide, BaC_2, according to this formula, the effective bond order of carbon atoms is '3', and formal charge is '-1'. Similarly, for $Me_n(C_3)_mC_k$ carbides containing only $[C_3]$ units, we used the following equation:

$$EBO = \frac{(3 \times 4m - nZ_{Me} + 4k)}{4m}. \quad (2)$$

The results of our calculations for the binary metal-carbon compounds found in the literature [17,29,54,67–84] are presented in the graphical form in Fig. S8, showing a correlation between the C–C distances in $[C_2]$ and $[C_3]$ units, d(C–C), and the bond order in the pairs of C atoms (green and blue dots). The data points shown by green and blue dots in Fig. S8 were fitted by the linear equation: $EBO = 10.81 - 6.57 \times d\,(C\text{–}C)$ (dashed line in Fig. S8).

With the linear equation obtained above, we determined the bond order for C–C bonds for all dysprosium carbides studied here, using the values of $d(C\text{–}C)$ obtained experimentally from SCXRD. For Dy_3C_2 we found the bond order ~1 in dimers, implying it to be an ethanide featuring $[C_2]^{6-}$ units, which is in perfect agreement with the reasoning presented in Ref. [29]. In dimers of γ-Dy_4C_5, the EBO is of ~1.71 (implying the formal charge of the dimers as $[C_2]^{4.6-}$), whereas in trimers the EBO is of ~1.40, suggesting $[C_3]^{6.4-}$ units. For Dy_5C_9, all C–C bonds in the chains are similar, and the EBO is of ~1.22 (thus one-dimensionally infinite polyanions $^1_\infty\left[(C_4)^{6.2-}\right]$). For γ-$DyC_2$, possessing ribbons of fused hexagon rings, the estimated C–C EBO is of ~1.27 for shared hexagon edges and of ~0.90 for unshared ones. This gives a formal charge of ~ −3.0 for two carbons per formula unit. Remarkably, the same reasoning implies a formal charge of ~ −2.4 per two carbon atoms in HP-CaC_2 [28], that is about 1e less than expected for Ca^{2+} vs Dy^{3+}. Knowing the EBO (thus formal charges) of the carbon polyanions, we can estimate the oxidation state of dysprosium atoms in the studied compounds: dysprosium (III) in γ-DyC_2, Dy_5C_9, γ-Dy_4C_5, and Dy_4C_3, and dysprosium (II) in Dy_3C_2.

The Mulliken charges of dysprosium in the carbides at ~70 GPa were found to be 1.66 for Dy1 in γ-DyC_2; 1.88 for Dy1 and Dy2 in Dy_5C_9; 1.69 for Dy1, 1.75 for Dy2 and 1.55 for Dy3 in γ-Dy_4C_5; 1.01 for Dy1 and 1.13 for Dy2 in Dy_3C_2; and 1.64 for Dy in Dy_4C_3 (Table S9). The values for γ-DyC_2, Dy_5C_9, γ-Dy_4C_5, and Dy_4C_3 are consistent with the Mulliken charges reported for other dysprosium(III)-containing compounds [29,85,86]. The lower Mulliken charges of dysprosium in Dy_3C_2 are in agreement with the assessment of the cation in this compound as Dy^{2+} [29]. The model Y–C system shows similar results (Table S10).

Experimental studies of the equations of state of dysprosium carbides were beyond the scope of this work, however the pressure-volume relations were simulated and described with the second order Birch-Murnaghan equation of state (Table S11). The calculated bulk moduli decrease with an increase in dysprosium content and a simultaneous decrease in the number of homoatomic bonds in carbon anions, progressing from carbon ribbons, chains, trimers, and dumbbells to discrete carbon atoms, as follows: K_0(γ-DyC_2) = 189(2) GPa > K_0(Dy_5C_9) = 164 (2) GPa > K_0(γ-Dy_4C_5) = 123.8(8) GPa > K_0(Dy_3C_2) = 96.7(9) GPa > K_0(Dy_4C_3) = 91.6(1.2) GPa (Table S11, Fig. S9). Although the dysprosium content in Dy_4C_3 is slightly less than in Dy_3C_2, its bulk modulus is relatively lower. This is likely due to the different nature of carbon anions: Dy_3C_2 contains carbon dumbbells, whereas the structure of Dy_4C_3 features discrete carbon atoms. There is also an inverse correlation between the compressibility and the ratio $R = <d>^3/(Z_{Dy}{}^*Z_C)$ ($<d>$ is the average Dy–C distance in the first coordination sphere; Z_{Dy} and Z_C are the formal charges of dysprosium and carbon) (Fig. S10a). For the studied compounds, with the increase of the R ratio the compressibility decreases (Fig. S10a), whereas for ionic and ionic-covalent compounds the correlation is known to be direct [3,87]. This indicates an unusual compression mechanism for the studied dysprosium carbides that is in line with the observation of the almost linear correlation between compressibility and the average bond order in carbon pairs (Fig. S10b).

Computations of phonon dispersion relations in harmonic approximation at 0 K show that at 70 GPa γ-DyC_2, Dy_5C_9, γ-Dy_4C_5 and Dy_4C_3 exhibit dynamical stability (Fig. S11), while Dy_3C_2 shows tiny instability at 70 GPa (Fig. S11g) similar to that found previously for this compound at the synthesis pressure of 55 GPa [29]. γ-DyC_2, γ-Dy_4C_5 and Dy_4C_3 are predicted to be dynamically stable at 0 GPa (Figs. S11b, f, j) and thus potentially quenchable to ambient conditions, but one should consider this prediction with caution. Notably, γ-Y_4C_5 discovered earlier was found dynamically unstable at ambient conditions [17] in contrast to the isostructural γ-Dy_4C_5 from the current study (Fig. S11f).

The calculated convex hull diagram at 0 K and 70 GPa (Fig. 3) shows that according to the theory, γ-DyC_2, γ-Dy_4C_5 and Dy_3C_2 are thermodynamically stable at the synthesis pressure. Two dysprosium carbides, Dy_5C_9 and Dy_4C_3, lie above the convex hull by 70 and 16 meV per atom, respectively (Fig. 3). These differences in energy turn out to be smaller than k_BT (241 meV) at the synthesis temperature (~2800 K), thus suggesting that these phases might be metastable at ambient temperature and high pressures.

4. Conclusion

To summarize, novel dysprosium carbides γ-DyC_2, Dy_5C_9, γ-Dy_4C_5, Dy_3C_2, and Dy_4C_3 were synthesized by the direct reaction of metallic dysprosium and carbon originated from diamond anvils upon laser heating to ~2800 K at ~70 GPa. Their crystal structures were studied *in situ*. The most notable features of the new carbides are polyacene-like ribbons in γ-DyC_2 and *cis*-polyacetylene-type chains in Dy_5C_9. This study demonstrates the drastic effect of high pressures on the chemistry of the Dy–C system with the general tendency to formation of carbides with complex polyanions.

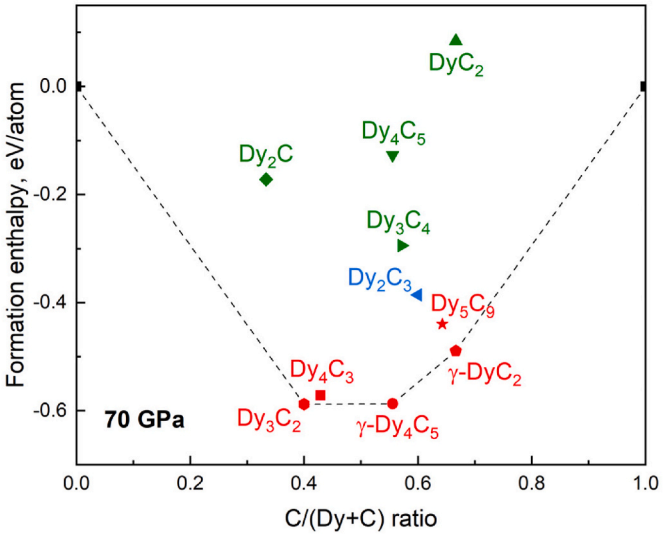

Fig. 3. Calculated convex hull diagram constructed for the Dy–C binary system at 70 GPa. Only known Dy–C phases are included. Dashed lines indicate the convex hull; carbides synthesized in this work are given in red; Dy_2C_3 (shown in blue) has been previously observed both at extreme [29] and ambient conditions [84]; carbides shown in green have been reported at ambient pressure (Dy_2C [88], Dy_4C_5 [73,89,90], Dy_3C_4 [91,92], and DyC_2 [54]). (A colour version of this figure can be viewed online.)

Data availability

The details of the crystal structure investigations may be obtained from The Cambridge Crystallographic Data Centre (CCDC, https://www.ccdc.cam.ac.uk/structures/) by quoting the deposition numbers 2311063, 2311064, 2311065, 2311066, and 2311067. All other information is available in the main text or the Supplementary materials.

CRediT authorship contribution statement

Fariia Iasmin Akbar: Writing – original draft, Visualization, Validation, Methodology, Investigation, Conceptualization. **Alena Aslandukova:** Methodology, Investigation. **Yuqing Yin:** Investigation. **Andrey Aslandukov:** Writing – review & editing, Investigation. **Dominique Laniel:** Writing – review & editing, Investigation. **Elena Bykova:** Investigation. **Maxim Bykov:** Writing – review & editing, Investigation. **Eleanor Lawrence Bright:** Resources, Methodology. **Jonathan Wright:** Resources, Methodology. **Davide Comboni:** Resources, Methodology. **Michael Hanfland:** Resources, Methodology. **Natalia Dubrovinskaia:** Writing – review & editing, Supervision, Conceptualization. **Leonid Dubrovinsky:** Writing – review & editing, Validation, Supervision, Methodology, Conceptualization.

Declaration of competing interest

The authors declare that they have no known competing financial interests or personal relationships that could have appeared to influence the work reported in this paper.

Acknowledgements

The authors acknowledge the European Synchrotron Radiation Facility (ESRF) for the provision of beamtime at the ID15b and ID11 beamlines. Computations were performed at the Leibniz Supercomputing Center of the Bavarian Academy of Sciences and the Humanities, and the research center for scientific computing at the University of Bayreuth. F.I.A., N.D., and L.D. thank Gerd Steinle-Neumann (Bavarian Research Institute of Experimental Geochemistry and Geophysics (BGI), University of Bayreuth, 95440 Bayreuth, Germany) for the valuable discussions and advice regarding the theoretical calculations. N.D. and L.D. thank the Deutsche Forschungsgemeinschaft (DFG projects DU 393–9/2, DU 393–13/1; DU 945/15–1; LA 4916/1-1) for financial support. N.D. also thanks the Swedish Government Strategic Research Area in Materials Science on Functional Materials at Linköping University (Faculty Grant SFO-Mat-LiU No. 2009 00971). M. B. acknowledges the support of Deutsche Forschungsgemeinschaft (DFG Emmy-Noether Program project BY112/2–1). Co-funded by the European Union (ERC, HIPMAT, 101077963). Views and opinions expressed are however those of the author(s) only and do not necessarily reflect those of the European Union or the European Research Council. Neither the European Union nor the granting authority can be held responsible for them. D.L. thanks the UKRI Future Leaders Fellowship (MR/V025724/1) for financial support. For the purpose of open access, the author has applied a Creative Commons Attribution (CC BY) license to any Author Accepted Manuscript version arising from this submission.

Appendix A. Supplementary data

Supplementary data to this article can be found online at https://doi.org/10.1016/j.carbon.2024.119374.

References

[1] Y. Yin, A. Aslandukova, N. Jena, F. Trybel, I.A. Abrikosov, B. Winkler, et al., Unraveling the bonding complexity of polyhalogen anions: high-pressure synthesis of unpredicted sodium chlorides Na_2Cl_3 and Na_4Cl_5 and bromide Na_4Br_5, JACS Au 3 (2023) 1634–1641, https://doi.org/10.1021/jacsau.3c00090.

[2] W. Zhang, A.R. Oganov, A.F. Goncharov, Q. Zhu, S.E. Boulfelfel, A.O. Lyakhov, et al., Unexpected stable stoichiometries of sodium chlorides, Science 342 (2013) 1502–1505, https://doi.org/10.1126/science.1244989.

[3] D. Laniel, B. Winkler, T. Fedotenko, A. Aslandukova, A. Aslandukov, S. Vogel, et al., High-pressure $Na_3(N_2)_4$, $Ca_3(N_2)_4$, $Sr_3(N_2)_4$, and $Ba(N_2)_3$ featuring nitrogen dimers with noninteger charges and anion-driven metallicity, Phys. Rev. Mater. 6 (2022) 023402, https://doi.org/10.1103/PhysRevMaterials.6.023402.

[4] A. Aslandukov, F. Trybel, A. Aslandukova, D. Laniel, T. Fedotenko, S. Khandarkhaeva, et al., Anionic N_{18} macrocycles and a polynitrogen double helix in novel yttrium polynitrides YN_6 and Y_2N_{11} at 100 GPa, Angew. Chem. Int. Ed. 61 (2022) e202207469, https://doi.org/10.1002/anie.202207469.

[5] M. Bykov, E. Bykova, G. Aprilis, K. Glazyrin, E. Koemets, I. Chuvashova, et al., Fe-N system at high pressure reveals a compound featuring polymeric nitrogen chains, Nat. Commun. 9 (2018) 2756, https://doi.org/10.1038/s41467-018-05143-2.

[6] A. Aslandukov, A. Aslandukova, D. Laniel, S. Khandarkhaeva, Y. Yin, F.I. Akbar, et al., Stabilization of N_6 and N_8 anionic units and 2D polynitrogen layers in high-pressure scandium polynitrides, Nat. Commun. 15 (2024) 2244, https://doi.org/10.1038/s41467-024-46313-9.

[7] B.A. Steele, E. Stavrou, J.C. Crowhurst, J.M. Zaug, V.B. Prakapenka, I.I. Oleynik, High-pressure synthesis of a pentazolate salt, Chem. Mater. 29 (2017) 735–741, https://doi.org/10.1021/acs.chemmater.6b04538.

[8] D. Laniel, F. Trybel, Y. Yin, T. Fedotenko, S. Khandarkhaeva, A. Aslandukov, et al., Aromatic hexazine $[N_6]^{4-}$ anion featured in the complex structure of the high-pressure potassium nitrogen compound K_9N_{56}, Nat. Chem. 15 (2023) 641–646, https://doi.org/10.1038/s41557-023-01148-7.

[9] Y. Wang, M. Bykov, I. Chepkasov, A. Samtsevich, E. Bykova, X. Zhang, et al., Stabilization of hexazine rings in potassium polynitride at high pressure, Nat. Chem. 14 (2022) 794–800, https://doi.org/10.1038/s41557-022-00925-0.

[10] N.P. Salke, K. Xia, S. Fu, Y. Zhang, E. Greenberg, V.B. Prakapenka, et al., Tungsten hexanitride with single-bonded armchairlike hexazine structure at high pressure, Phys. Rev. Lett. 126 (2021) 065702, https://doi.org/10.1103/PhysRevLett.126.065702.

[11] Y. Zhang, L. Wu, B. Wan, Y. Zhao, R. Gao, Z. Li, et al., Structural variety beyond appearance: high-pressure phases of CrB_4 in comparison with FeB_4, Phys. Chem. Chem. Phys. 18 (2016) 2361–2368, https://doi.org/10.1039/c5cp06745f.

[12] E. Bykova, E. Johansson, M. Bykov, S. Chariton, H. Fei, S.V. Ovsyannikov, et al., Novel class of rhenium borides based on hexagonal boron networks interconnected by short B2Dumbbells, Chem. Mater. 34 (2022) 8138–8152, https://doi.org/10.1021/acs.chemmater.2c00520.

[13] A.P. Drozdov, P.P. Kong, V.S. Minkov, S.P. Besedin, M.A. Kuzovnikov, S. Mozaffari, et al., Superconductivity at 250 K in lanthanum hydride under high pressures, Nature 569 (2019) 528–531, https://doi.org/10.1038/s41586-019-1201-8.

[14] D. Laniel, B. Winkler, E. Bykova, T. Fedotenko, S. Chariton, V. Milman, et al., Novel sulfur hydrides synthesized at extreme conditions, Phys. Rev. B 102 (2020) 134109, https://doi.org/10.1103/PhysRevB.102.134109.

[15] V.V. Struzhkin, D.Y. Kim, E. Stavrou, T. Muramatsu, H.K. Mao, C.J. Pickard, et al., Synthesis of sodium polyhydrides at high pressures, Nat. Commun. 7 (2016) 12267, https://doi.org/10.1038/ncomms12267.

[16] M. Miao, Y. Sun, E. Zurek, H. Lin, Chemistry under high pressure, Nat. Rev. Chem 4 (2020) 508–527, https://doi.org/10.1038/s41570-020-0213-0.

[17] A. Aslandukova, A. Aslandukov, L. Yuan, D. Laniel, S. Khandarkhaeva, T. Fedotenko, et al., Novel high-pressure yttrium carbide γ-Y_4C_5 containing $[C_2]$ and nonlinear $[C_3]$ units with unusually large formal charges, Phys. Rev. Lett. 127 (2021) 135501, https://doi.org/10.1103/PhysRevLett.127.135501.

[18] L. Wang, X. Dong, Y. Wang, H. Zheng, K. Li, X. Peng, et al., Pressure-Induced polymerization and disproportionation of Li_2C_2 accompanied with irreversible conductivity enhancement, J. Phys. Chem. Lett. 8 (2017) 4241–4245, https://doi.org/10.1021/acs.jpclett.7b01779.

[19] X. Dong, L. Wang, K. Li, H. Zheng, Y. Wang, Y. Meng, et al., Tailored synthesis of the narrowest zigzag graphene nanoribbon structure by compressing the lithium acetylide under high temperature, J. Phys. Chem. C 122 (2018) 20506–20512, https://doi.org/10.1021/acs.jpcc.8b04081.

[20] Y.L. Li, S.N. Wang, A.R. Oganov, H. Gou, J.S. Smith, T.A. Strobel, Investigation of exotic stable calcium carbides using theory and experiment, Nat. Commun. 6 (2015) 6974, doi:10.1038/ncomms7974.

[21] C. Su, J. Zhang, G. Liu, X. Wang, H. Wang, Y. Ma, Catenation of carbon in LaC_2 predicted under high pressure, Phys. Chem. Chem. Phys. 18 (2016) 14286–14291, https://doi.org/10.1039/c6cp01484d.

[22] Y. Guo, C. Yu, J. Lin, C. Wang, C. Ren, B. Sun, et al., Pressure-induced structural transformations and polymerization in ThC_2, Sci. Rep. 7 (2017) 45872, https://doi.org/10.1038/srep45872.

[23] X. Feng, S. Lu, C.J. Pickard, H. Liu, S.A.T. Redfern, Y. Ma, Carbon network evolution from dimers to sheets in superconducting ytrrium dicarbide under pressure, Commun. Chem. 1 (2018) 85, https://doi.org/10.1038/s42004-018-0085-0.

[24] J. Nylén, S. Konar, P. Lazor, D. Benson, U. Häussermann, Structural behavior of the acetylide carbides Li_2C_2 and CaC_2 at high pressure, J. Chem. Phys. 137 (2012) 224507, https://doi.org/10.1063/1.4770268.

[25] M. Debessai, J.J. Hamlin, J.S. Schilling, D. Rosenmann, D.G. Hinks, H. Claus, Superconductivity for CaC_6 to 32 GPa hydrostatic pressure, Phys. Rev. B Condens. Matter 82 (2010) 132502, https://doi.org/10.1103/PhysRevB.82.132502.

[26] A. Gauzzi, S. Takashima, N. Takeshita, C. Terakura, H. Takagi, N. Emery, et al., Enhancement of superconductivity and evidence of structural instability in intercalated graphite CaC6 under high pressure, Phys. Rev. Lett. 98 (2007) 067002, https://doi.org/10.1103/PhysRevLett.98.067002.

[27] L. Zhang, Y. Xie, T. Cui, Y. Li, Z. He, Y. Ma, et al., Pressure-induced enhancement of electron-phonon coupling in superconducting CaC_6 from first principles, Phys. Rev. B Condens. Matter 74 (2006) 184519, https://doi.org/10.1103/PhysRevB.74.184519.

[28] S. Khandarkhaeva, T. Fedotenko, A. Aslandukova, F.I. Akbar, M. Bykov, D. Laniel, et al., Extending carbon chemistry at high-pressure by synthesis of CaC_2 and Ca_3C_7 with deprotonated polyacene- and para-poly(indenoindene)-like nanoribbons, Nat. Commun. 15 (2024) 2855, https://doi.org/10.1038/s41467-024-47138-2.

[29] F.I. Akbar, A. Aslandukova, A. Aslandukov, Y. Yin, F. Trybel, S. Khandarkhaeva, et al., High-pressure synthesis of dysprosium carbides, Front. Chem. 11 (2023) 1–9, https://doi.org/10.3389/fchem.2023.1210081.

[30] I. Kantor, V. Prakapenka, A. Kantor, P. Dera, A. Kurnosov, S. Sinogeikin, et al., BX90: a new diamond anvil cell design for X-ray diffraction and optical measurements, Rev. Sci. Instrum. 83 (2012) 125102, https://doi.org/10.1063/1.4768541.

[31] T. Fedotenko, L. Dubrovinsky, G. Aprilis, E. Koemets, A. Snigirev, I. Snigireva, et al., Laser heating setup for diamond anvil cells for in situ synchrotron and in house high and ultra-high pressure studies, Rev. Sci. Instrum. 90 (2019) 104501, https://doi.org/10.1063/1.5117786.

[32] P.I. Dorogokupets, A. Dewaele, Equations of state of MgO, Au, Pt, NaCl-B1, and NaCl-B2: internally consistent high-temperature pressure scales, High Pres. Res. 27 (2007) 431–446, https://doi.org/10.1080/08957950701659700.

[33] T. Sakai, E. Ohtani, N. Hirao, Y. Ohishi, Equation of state of the NaCl-B2 phase up to 304 GPa, J. Appl. Phys. 109 (2011) 084912, https://doi.org/10.1063/1.3573393.

[34] R. Hrubiak, J.S. Smith, G. Shen, Multimode scanning X-ray diffraction microscopy for diamond anvil cell experiments, Rev. Sci. Instrum. 90 (2019) 025109, doi: 10.1063/1.5057518.

[35] Rigaku Oxford Diffraction, CrysAlisPro Software system, 2015, https://doi.org/10.1063/1.2372734.

[36] A. Aslandukov, M. Aslandukov, N. Dubrovinskaia, L. Dubrovinsky, Domain Auto Finder (DAFi) program: the analysis of single-crystal X-ray diffraction data from polycrystalline samples, J. Appl. Crystallogr. 55 (2022) 1383–1391, https://doi.org/10.1107/s1600576722008081.

[37] O.V. Dolomanov, L.J. Bourhis, R.J. Gildea, J.A.K. Howard, H. Puschmann, OLEX2: a complete structure solution, refinement and analysis program, J. Appl. Crystallogr. 42 (2009) 339–341, https://doi.org/10.1107/S0021889808042726.

[38] G.M. Sheldrick, SHELXT – integrated space-group and crystal-structure determination, Acta Crystallogr. Sect. A Found. Adv. 71 (2015) 3–8, https://doi.org/10.1107/S2053273314026370.

[39] G.M. Sheldrick, Crystal structure refinement with SHELXL, Acta Crystallogr., Sect. C: Struct. Chem. 71 (2015) 3–8, https://doi.org/10.1107/S2053229614024218.

[40] K. Momma, F. Izumi, VESTA 3 for three-dimensional visualization of crystal, volumetric and morphology data, J. Appl. Crystallogr. 44 (2011) 1272–1276, https://doi.org/10.1107/S0021889811038970.

[41] J. Gonzalez-Platas, M. Alvaro, F. Nestola, R. Angel, EosFit7-GUI: a new graphical user interface for equation of state calculations, analyses and teaching, J. Appl. Crystallogr. 49 (2016) 1377–1382, https://doi.org/10.1107/S1600576716008050.

[42] G. Kresse, J. Furthmüller, Efficiency of ab-initio total energy calculations for metals and semiconductors using a plane-wave basis set, Comput. Mater. Sci. 6 (1996) 15–50, https://doi.org/10.1016/0927-0256(96)00008-0.

[43] P.E. Blöchl, Projector augmented-wave method, Phys. Rev. B 50 (1994) 17953–17979, https://doi.org/10.1103/PhysRevB.50.17953.

[44] J.P. Perdew, K. Burke, M. Ernzerhof, Generalized gradient approximation made simple, Phys. Rev. Lett. 77 (1996) 3865–3868, https://doi.org/10.1103/PhysRevLett.77.3865.

[45] H.J. Monkhorst, J.D. Pack, Special points for Brillonin-zone integrations, Phys. Rev. B 13 (1976) 5188–5192, https://doi.org/10.1103/PhysRevB.13.5188.

[46] A. Togo, I. Tanaka, First principles phonon calculations in materials science, Scripta Mater. 108 (2015) 1–6, https://doi.org/10.1016/j.scriptamat.2015.07.021.

[47] J. Rath, A.J. Freeman, Generalized Magnetic Susceptibilities in Metals: Application of the Analytic Tetrahedron Linear Energy Method to Sc, Physical Review B 11 (1975) 2109–2117, https://doi.org/10.1103/PhysRevB.11.2109.

[48] C. Friedrich, Tetrahedron integration method for strongly varying functions: application to the GT self-energy, Phys. Rev. B 100 (2019) 075142, https://doi.org/10.1103/PhysRevB.100.075142.

[49] P.C. Müller, C. Ertural, J. Hempelmann, R. Dronskowski, Crystal orbital bond index: covalent bond orders in solids, J. Phys. Chem. C 125 (2021) 7959–7970, https://doi.org/10.1021/acs.jpcc.1c00718.

[50] S. Maintz, V.L. Deringer, A.L. Tchougréeff, R. Dronskowski, LOBSTER: a tool to extract chemical bonding from plane-wave based DFT, J. Comput. Chem. 37 (2016) 1030–1035, https://doi.org/10.1002/jcc.24300.

[51] L. Pauling, The principles determining the structure of complex ionic crystals, J. Am. Chem. Soc. 51 (1929) 1010–1026, https://doi.org/10.1021/ja01379a006.

[52] M. Nespolo, B. Guillot, CHARDI2015: charge distribution analysis of non-molecular structures, J. Appl. Crystallogr. 49 (2016) 317–321, https://doi.org/10.1107/S1600576715024814.

[53] Deposition Numbers 2311063, 2311064, 2311065, 2311066, and 2311067 contain the supplementary crystallographic data for this paper. These data are provided free of charge by the joint Cambridge Crystallographic Data Centre and Fachinformationszentrum Karlsruhe Access Structures service via www.ccdc.cam.ac.uk/structures.

[54] G.Y. Adachi, Y. Shibata, K. Ueno, J. Shiokawa, Heats of the tetragonal-cubic transformation in rare earth dicarbides and mixed rare earth dicarbide solid solutions, J. Inorg. Nucl. Chem. 38 (1976) 1023–1026, https://doi.org/10.1016/0022-1902(76)80021-8.

[55] V. Babizhetskyy, B. Kotur, V. Levytskyy, H. Michor, Alloy systems and compounds containing rare earth metals and carbon, Handb. Phys. Chem. Rare Earths 52 (2017) 1–263, https://doi.org/10.1016/bs.hpcre.2017.09.001.

[56] R. Vidhya, M.P. Antony, P.R. Vasudeva Rao, Enthalpy and Gibbs energy of formation of dysprosium dicarbide, J. Nucl. Mater. 350 (2006) 129–134, https://doi.org/10.1016/j.jnucmat.2005.12.001.

[57] H.P. Sarker, M.N. Huda, Role of f-electrons in determining insulator to metal phase transitions of $Ca(La_{1-x}Ce_x)_2S_4$ ($0 \leq x \leq 1$) solid solution: a DFT + U study, J. Appl. Phys. 130 (2021) 145102, https://doi.org/10.1063/5.0058096.

[58] N. Tateiwa, J. Pospíšil, Y. Haga, H. Sakai, T.D. Matsuda, E. Yamamoto, Itinerant ferromagnetism in actinide 5 f-electron systems: phenomenological analysis with spin fluctuation theory, Phys. Rev. B 96 (2017) 035125, https://doi.org/10.1103/PhysRevB.96.035125.

[59] J.E. Anthony, The larger acenes: versatile organic semiconductors, Angew. Chem. Int. Ed. 47 (2008) 452–483, https://doi.org/10.1002/anie.200604045.

[60] R.E. Newnham, Properties of materials: anisotropy, Symmetry, Structure (2005).

[61] Q. Ai, K. Jarolimek, S. Mazza, J.E. Anthony, C. Risko, Delimited polyacenes: edge topology as a tool to modulate carbon nanoribbon structure, conjugation, and mobility, Chem. Mater. 30 (2018) 947–957, https://doi.org/10.1021/acs.chemmater.7b04715.

[62] U. Ruschewitz, Binary and ternary carbides of alkali and alkaline-earth metals, Coord. Chem. Rev. 244 (2003) 115–136, https://doi.org/10.1016/S0010-8545(03)00102-4.

[63] X. Dong, A.R. Oganov, H. Cui, X.-F. Zhou, H.-T. Wang, Electronegativity and chemical hardness of elements under pressure, Proc. Natl. Acad. Sci. 119 (2022) 1–8, https://doi.org/10.1073/pnas.2117416119.

[64] M. Rahm, T. Zeng, R. Hoffmann, Electronegativity seen as the ground-state average valence electron binding energy, J. Am. Chem. Soc. 141 (2019) 342–351, https://doi.org/10.1021/jacs.8b10246.

[65] M. Rahm, R. Cammi, N.W. Ashcroft, R. Hoffmann, Squeezing all elements in the periodic table: electron configuration and electronegativity of the atoms under compression, J. Am. Chem. Soc. 141 (2019) 10253–10271, https://doi.org/10.1021/jacs.9b02634.

[66] C.S. Yannoni, T.C. Clarke, Molecular geometry of cis- and trans-polyacetylene by nutation NMR spectroscopy, Phys. Rev. Lett. 51 (1983) 1191–1193, https://doi.org/10.1103/PhysRevLett.51.1191.

[67] V. Vohn, W. Kockelmann, U. Ruschewitz, On the synthesis and crystal structure of BaC2, J. Alloys Compd. 284 (1999) 132–137, https://doi.org/10.1016/S0925-8388(98)00957-8.

[68] V. Vohn, M. Knapp, U. Ruschewitz, Synthesis and crystal structure of SrC_2, J. Solid State Chem. 151 (2000) 111–116, https://doi.org/10.1006/jssc.2000.8630.

[69] M. Atoji, Magnetic and crystal structures of CeC_2, PrC_2, NdC_2, TbC_2, and HoC_2 at low temperatures, J. Chem. Phys. 46 (1967) 1891–1901, https://doi.org/10.1063/1.1840950.

[70] M. Atoji, Neutron diffraction study of Ce_2C_3 at low temperatures, J. Chem. Phys. 46 (1967) 4148–4149, https://doi.org/10.1063/1.1840499.

[71] Y. Yosida, Surface superconductivity and structural analysis of YC_2 single crystals encapsulated in carbon nanocages, J. Appl. Phys. 92 (2002) 5494–5497, https://doi.org/10.1063/1.1510946.

[72] M.C. Krupka, A.L. Giorgi, N.H. Krikorian, E.G. Szklaizz, High-pressure synthesis of yttrium-thorium sesquicarbide: a new high-temeperature superconductor, J. Less Common. Met. 19 (1969) 113–119, https://doi.org/10.1016/0022-5088(69)90026-5.

[73] R. Czekalla, T. Hüfken, W. Jeitschko, R.D. Hoffmann, R. Pöttgen, The rare earth carbides R_4C_5 with R=Y, Gd, Tb, Dy, and Ho, J. Solid State Chem. 132 (1997) 294–299, https://doi.org/10.1006/jssc.1997.7461.

[74] M. Atoji, K. Gschneidner, A.H. Daane, R.E. Rundle, F.H. Spedding, The structures of lanthanum dicarbide and sesquicarbide by X-ray and neutron diffraction, J. Am. Chem. Soc. 80 (1958) 1804–1808, https://doi.org/10.1021/ja01541a008.

[75] R. Czekalla, W. Jeitschko, R.-D. Hoffmann, H. Rabeneck, Preparation, crystal structure, and properties of the lanthanoid carbides Ln_4C_7 with ln = Ho, Er, Tm, and Lu, Zeitschrift für Naturforschung B 51 (1996) 646–654, https://doi.org/10.1515/znb-1996-0505.

[76] H. Ninomiya, T. Koshinuma, T. Nishio, H. Fujihisa, K. Kawashima, I. Hase, et al., Experimental and computational determination of optimal boron content in layered superconductor $Sc_{20}C_{8-x}B_xC_{20}$, Inorg. Chem. 59 (2020) 14290–14295, https://doi.org/10.1021/acs.inorgchem.0c02090.

[77] T.W. Button, I.J. McColm, Reaction of carbon with lanthanide silicides IV: the Y_5Si_3-C system, J. Less Common. Met. 97 (1984) 237–244, https://doi.org/10.1016/0022-5088(84)90028-6.

[78] O. Reckeweg, A. Baumann, H.A. Mayer, J. Glaser, H.J. Meyer, On the coexistence of tetragonal and monoclinic CaC_2: structural and spectroscopic studies on alkaline earth metal acetylides, MC_2 (M = Ca, Sr, Ba), Zeitschrift für anorganische und allgemeine Chemie 625 (1999) 1686–1692, https://doi.org/10.1002/(sici)1521-3749(199910)625:10<1686::aid-zaac1686>3.3.co;2-o.

[79] K. Klöss, D. Hinz-Hübner, U. Ruschewitz, Über eine neue Modifikation des Na_2C_2, Z. Anorg. Allg. Chem. 628 (2002) 2701–2704, https://doi.org/10.1002/1521-3749(200212)628:12<2701::AID-ZAAC2701>3.0.CO;2-%23.

[80] S. Hemmersbach, B. Zibrowius, U. Ruschewitz, Na_2C_2 und K_2C_2: Synthese, Kristallstruktur und spektroskopische Eigenschaften, Z. Anorg. Allg. Chem. 625 (1999) 1440–1446, https://doi.org/10.1002/(SICI)1521-3749(199909)625.

[81] H. Fjellvåg, P. Karen, Crystal structure of magnesium sesquicarbide, Inorg. Chem. 31 (1992) 3260–3263, https://doi.org/10.1021/ic00041a018.

[82] P. Karen, A. Kjekshus, Q. Huang, V.L. Karen, The crystal structure of magnesium dicarbide, J. Alloys Compd. 282 (1999) 72–75, https://doi.org/10.1016/S0925-8388(98)00828-7.
[83] V. Babizhetskyy, O. Jepsen, R.K. Kremer, A. Simon, B. Ouladdiaf, A. Stolovits, Structure and bonding of superconducting LaC_2, J. Phys. Condens. Matter 26 (2014) 025701, https://doi.org/10.1088/0953-8984/26/2/025701.
[84] F.H. Spedding, K. Gschneidner Jr., A.H. Daane, The crystal structures of some of the rare earth carbides, J. Am. Chem. Soc. 80 (1958) 4499–4503, https://doi.org/10.1021/ja01550a017.
[85] T. Gupta, G. Velmurugan, T. Rajeshkumar, G. Rajaraman, Role of Lanthanide-Ligand bonding in the magnetization relaxation of mononuclear single-ion magnets: a case study on Pyrazole and Carbene ligated Ln^{III}(Ln=Tb, Dy, Ho, Er) complexes, J. Chem. Sci. 128 (2016) 1615–1630, https://doi.org/10.1007/s12039-016-1147-4.
[86] G. Ahuja, G. Arora, Study of electronic properties of Dy_2O_3 using first principles calculations, Int. J. Pure Appl. Phys. 13 (2017) 123–126.
[87] R.M. Hazen, L.W. Finger, Bulk modulus-volume relationship for cation-anion polyhedra, J. Geophys. Res. 84 (1979) 6723–6728, https://doi.org/10.1029/JB084iB12p06723.
[88] M. Atoji, Neutron-diffraction studies of Tb_2C and Dy_2C in the temperature range 4-296 K, J. Chem. Phys. 75 (1981) 1434–1441, https://doi.org/10.1063/1.442150.
[89] The Materials Project, Materials Data on Dy_4C_5 by Materials Project, 2020, https://doi.org/10.17188/1664795. United States.
[90] V. Babizhetskyy, B. Kotur, V. Levytskyy, Phase equilibria and crystal structure of the ternary compounds in Dy–B–C system at 1270 K, Proc. Shevchenko Sci. Soc. Chem. Sci. LVI (2019) 45–55, https://doi.org/10.37827/ntsh.chem.2019.56.045.
[91] T. Hüfken, W. Jeitschko, The high-temperature (β) modification of Y_4C_7 with Lu_4C_7 type and Dy_3C_4 with Sc_3C_4 type structure, J. Alloys Compd. 278 (1998) 161–164, https://doi.org/10.1016/S0925-8388(98)00541-6.
[92] The Materials Project, Materials Data on Dy_3C_4 by Materials Project, 2020, https://doi.org/10.17188/1665344. United States.